Optical Materials 96 (2019) 109348

Contents lists available at ScienceDirect

Optical Materials

journal homepage: www.elsevier.com/locate/optmat

Optoelectronic properties of hybrid diodes based on vanadyl-phthalocyanine and zinc oxide nanorods thin films

M. Raveendra Kiran[a,b,*], Hidayath Ulla[b,1], M.N. Satyanarayan[b], G. Umesh[b]

[a] Department of Physic, Vignan's Institute of Information Technology, Visakhapatnam, 530046, India
[b] Optoelectronics Laboratory, Department of Physics, National Institute of Technology Karnataka, Mangalore, 57502, India

ARTICLE INFO

Keywords:
Hybrid photodiodes
Impedance spectroscopy
Mobility
Responsivity
Charge transport

ABSTRACT

Herein, we report the optoelectronic properties of hybrid diodes fabricated using vanadyl phthalocyanine (VOPc) and zinc oxide nanorods (ZNR) with the configuration: ITO/ZNR/VOPc/MoO_3/Al. Vertically aligned ZnO nanorods were grown using a simple aqueous solution (AS) method as a function of growth temperature. The correlation between the morphology of ZNR films and the optoelectronic properties of the ZNR/VOPc hybrid devices was investigated. The results show that the hybrid diodes with ZNR films grown at 120 °C offer the best optoelectronic properties. The higher photocurrent responsivity, $R_{ph,}$ (16.28 A/W) was achieved for devices with ZNR films grown at 120 °C. This value is 25 times higher than the R_{ph} value obtained for the devices made with ZnO nanoparticle films that were reported earlier.

1. Introduction

Recently, organic-inorganic p-n junctions have simulated much attraction due to their possible applications in the field optoelectronics [1–5]. We have seen in our previous work that the morphology of the films plays a significant role in enhancing the performance of organic-inorganic photodiodes [6]. By utilizing the advantages of the individual material properties, such as high charge carrier mobility and environmental stability, these hybrid p-n junctions can minimize several factors that limit the performance of the devices. Several research groups have explored hybrid p-n interfaces of zinc oxide (ZnO) nanostructures with organic semiconductor materials due to their potential applications in miniature devices [7–11]. Due to the simple synthesis process, superior optical and electrical properties, able to form different nanostructures even at low temperatures (< 100 °C), ZnO nano-thin films have been widely exploited by forming hybrid junctions [12–14].

On the other hand, phthalocyanines have emerged as important materials for optoelectronic device applications [15]. Wide varieties of phthalocyanines (greater than 70) were synthesized, and several phthalocyanines were investigated for their structural, optical, electrical and photovoltaic properties [16–21]. Furthermore, it is observed from recent literature that the non-planar MPcs showed better stability and higher mobility than other phthalocyanines [22–25]. Also, non-planar phthalocyanine-based devices offer better performance in comparison with planar phthalocyanines [26–28]. Among many phthalocyanines, titanyl phthalocyanine (TiOPc) and vanadyl phthalocyanine (VOPc) are least investigated materials with regard to their electrical and photovoltaic properties.

Since a p-n junction is the fundamental component of any optoelectronic device, it is essential to understand the charge carrier dynamics at such hetero-junctions. Further, we have studied the devices made using ZnO nanorod (ZNR) films instead of ZnO nanoparticle films, which form a p-n junction with organic metal phthalocyanine (MPc) films. The heterojunction devices based on ZnO nanoparticles/MPcs such as ZnO/Zinc phthalocyanine [29–31], ZnO/Copper phthalocyanine [9,31–33], ZnO/tetra-sulfonated copper-phthalocyanine [34], ZnO/Nickel phthalocyanine [35], ZnO/cobalt phthalocyanine [33,36], have been well studied for photovoltaic applications. However, the devices based on ZNR/MPcs have not been explored much. Mainly, devices having a heterojunction of MPc film and ZNR (vertically aligned) film and/or ZNR film prepared by aqueous solution growth have been rarely studied. The influence of the growth parameters of vertically aligned nanorods film on the ZNR/MPc heterojunction also needs to be studied.

In our previous reports, we have shown that VOPc films deposited at lower rate acquire improved charge carrier mobilities [37]. It is also shown that the ZnO nanoparticle films, annealed at 350 °C, exhibit better optoelectronic properties in hybrid diodes based on ZnO and

* Corresponding author. Department of Physic, Vignan's Institute of Information Technology, Visakhapatnam, 530046, India.
E-mail address: kiran.phy85@gmail.com (M. Raveendra Kiran).
[1] Current address: National Centre for Flexible Electronics, Indian Institute of Technology Kanpur, Kanpur- 208016, India.

https://doi.org/10.1016/j.optmat.2019.109348
Received 3 July 2019; Received in revised form 10 August 2019; Accepted 22 August 2019

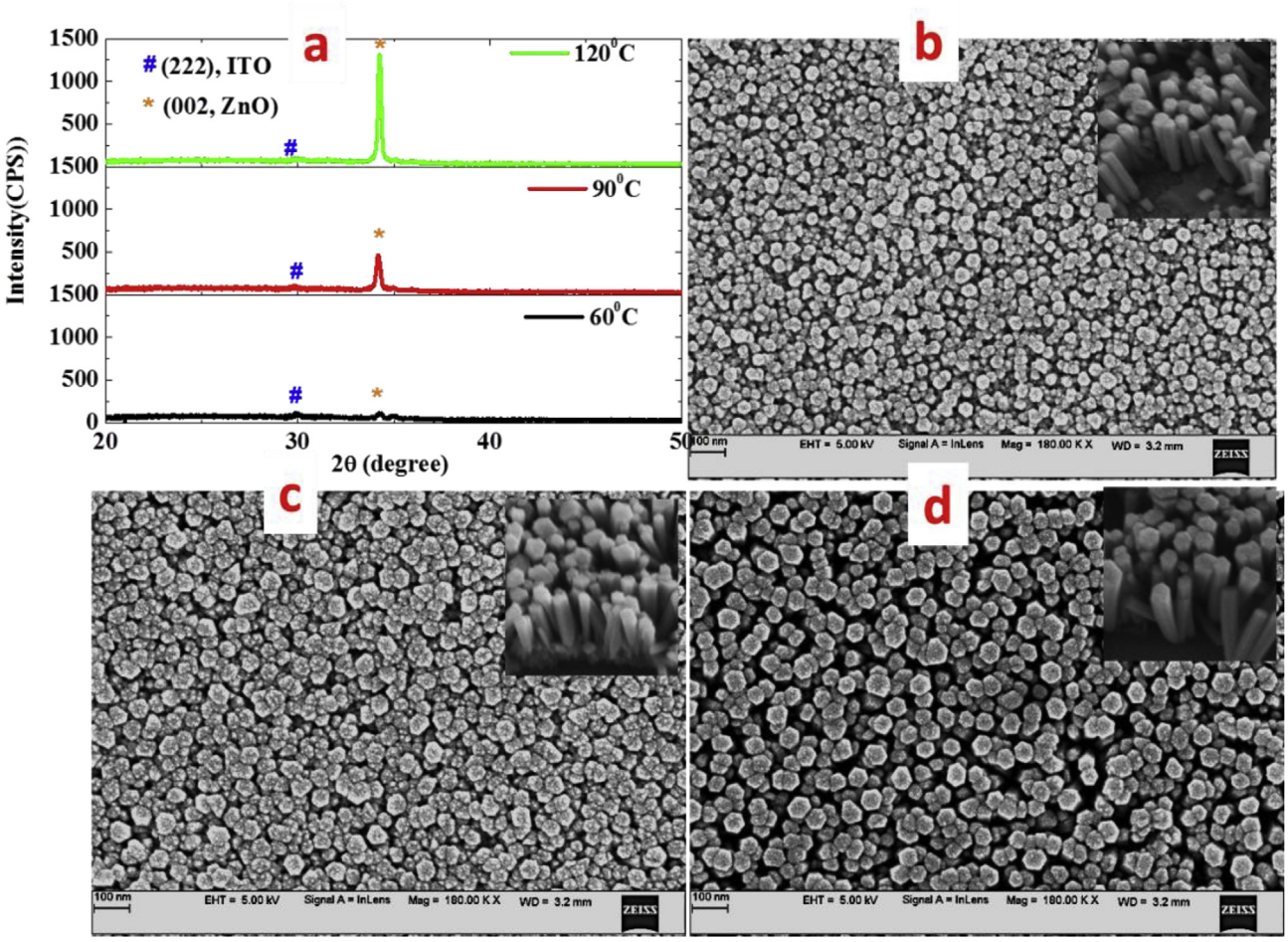

Fig. 1. (a) X-ray diffraction pattern of ZNR thin films grown at different temperatures; **(b)** SEM image of ZNR film grown at 60 °C, **(c)** at 90 °C and **(d)**at 120 °C for about 1 h (scale is 100 nm); insets show the columnar structures that confirm the vertical growth perpendicular to the plane of ITO substrate.

VOPc thin films [37]. However, to the best of our knowledge, the hybrid devices based on ZNR/VOPc have not been investigated extensively so far.

In this study, the optoelectronic properties of hybrid diodes involving ZNR and VOPc films are investigated as a function of nanorod growth temperature. We first investigated the effect of growth temperature on the structural, morphological and optical properties of the ZNR thin films. Subsequently, we also fabricated and performed interface measurements of p-n junction devices with the configuration: ITO/ZNR/VOPc/MoO_3/Al, under dark and illuminated conditions. These studies were carried out with the motivation to understand the charge carrier dynamics at ZNR/VOPc interfaces and their effect on charge carrier transport.

2. Experimental

2.1. Preparation of ZNR thin films and fabrication

The preparation of ZNR thin films was done in two steps, namely, (i) seed layer deposition and (ii) nanorod growth. The details of these steps are described below.

2.1.1. Preparation of seed layer thin films

The nanoparticulate seed layer thin films of ZnO were prepared using sol-gel spin coating techniques as described earlier in our previous reports [6,38]. 4 g of zinc acetate dehydrate [Zn $(CH3COO)_2{\cdot}2H_2O$] dissolved in 50 ml of 2-methoxy ethanol used as a precursor solution. This unsaturated solution was stirred on a preheated hot plate (kept at 70 °C) for 1 h. Monoethanolamine (MEA; 10 ml, acts as a stabilizer) was added drop-wise for about 10min, and the mixture was left stirring for about 2 h. The obtained clear solution was aged for 48 h to form a gel (at room temperature). The prepared sol-gel was spin-coated at a spin rate of 500 rpm for the first 30s, and then 100 rpm for next 30s on pre-cleaned ITO coated glass substrates. The spin-coated films were baked at 120 °C in a hot air oven for 10 min to remove the solvents.

2.1.2. Growth of ZNR thin films

To grow the ZnO nanorods, an aqueous solution (1:1) of 0.06 M zinc nitrate hexahydrate and hexamethyl tetra-amine was prepared in a glass reagent bottle (GL 45, BOROSIL). This served as the precursor solution. The substrates with pre-coated ZnO seed layer thin film were dipped vertically into the precursor solution in the bottle and kept in an oven at the desired temperature. After 1 h, the substrate was taken out and cleaned thoroughly multiple times with distilled water and further annealed at 350 °C for about 60 min. This process yielded ZnO nanorod thin film with nanorods aligned vertically to the surface of the substrate. These films were characterized in terms of their structural, morphological and optical properties.

The aqueous solution (AS) method employed in this work is a simple and less expensive technique, allowing one to grow uniform vertically aligned nanorods on a large scale at low temperatures. In the present work, we have grown the nanorods at three different temperatures viz., 60 °C, 90 °C and 120 °C. We were not able to proceed beyond 120 °C due to rapid evaporation of the solvent.

2.1.3. Fabrication of hybrid photodiode

The 100 nm thick VOPc layer was deposited on the pre-coated ZNR films using thermal evaporation method (at a base pressure of 8×10^{-6} mbar) at an evaporation rate of 0.1–0.2 Å/s. Next, to facilitate hole transport, a thin layer of molybdenum oxide (MoO_3, 3 nm) was deposited over the VOPc layer (at an evaporation rate of 0.1–0.2 Å/s). Finally, the aluminium layer (Al, a 100 nm thick) was deposited over the MoO_3 layer to function as a top electrode.

3. Results and discussion

3.1. Structural and morphological properties

The XRD pattern of the ZNR thin films grown on ITO coated glass substrate at different temperatures is shown in Fig. 1(a). The patters indicate that all the ZNR films are crystallized in hexagonal wurtzite structure [JCPDS 36–1451]. The intense peak appearing at 2θ = 34.2° is assigned to (002) crystal plane, which indicates that almost all the nanorods are oriented parallel to the c-axis. Further, the peak intensity is found to increase with growth temperature. A less intense peak also appears in the XRD pattern of each sample at 2θ = 30.2°, and this is ascribed to the ITO film [39,40]. The average crystallite size was estimated using Scherrer's formula and is found to increase from 31 nm to 50 nm as the growth temperature increases from 60 °C to 120 °C. The results are presented in Table 1.

The SEM images of nanorod thin film grown at different temperatures on ITO substrates are shown in Fig. 1(b–d). It shows that all the ZnO nanorods are oriented nearly perpendicular to the substrate plane regardless of growth temperature. The top view of SEM images reveals that the nanorods have a hexagonal shape, suggesting that the nanorods grew along the (002) direction at various temperatures. However, the diameter, as well as the length of the nanorods, was found to increase with an increase in the temperature of the precursor solution. In this connection, we utilize Image J and SPIP software to estimate nanorod diameter and length and the average spacing between the rods. The detailed analysis is presented as supplementary of this manuscript. It is observed that the average diameter of the nanorods increases from 38 nm to 60 nm, with an increase in the growth temperature from 60 °C to 120 °C. It is also observed that the inter nanorod gap increases from 56 nm to 74 nm with the increase in growth temperature. Further, the length of the nanorods is seen to increase by about 47% from ~150 nm to ~280 nm as the growth temperature increases from 60 °C to 120 °C. The results are tabulated in Table 1.

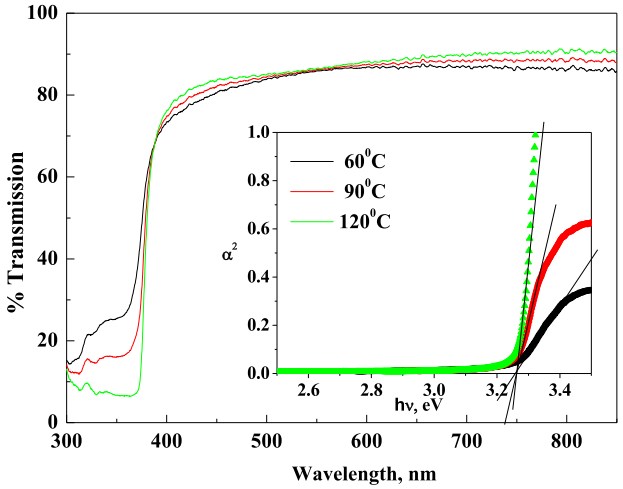

Fig. 2. Optical transmission spectra of ZNR films at different growth temperatures. The inset shows Tauc's plots to estimate bandgap of ZNR films at different growth temperature.

3.2. Optical transmission spectra

The optical transmission spectra of ZNR films grown at different temperatures are shown in Fig. 2. It is seen that all the samples show a transmission higher than 80% in the visible region. The plot of α^2 versus $h\nu$ for ZNR films grown at different temperatures is shown in the inset of Fig. 2. The optical band gap (E_g) values were estimated by extrapolating the straight-line portion of the plot to the x-axis and were found to be ~3.24 eV for all the samples [41]. These high transmissions of ZNR thin films (> 80%) are much needed to obtaining high photo responsivity. However, the transparency of the ZnO seed layer films exhibited grater transmission than the nanorod films as reported earlier [42].

3.3. J-V characteristics

The schematic of the proposed p-n hybrid diode is shown in Fig. 3(a), and its energy level diagram is shown in Fig. 3(b). The energy level values of the materials used in the devices have been taken from our previous work and the reported literature [6,36]. The J-V characteristics of p-n junctions involving ZNR films, grown at various

Table 1
Estimated p-n junction parameters from J-V characteristics.

T (⁰C)[a]	S (nm)[b]	D (nm)[c]	L (nm)[d]	X (nm)[e]	Condition	n[f]	Io (amp)[g]	V_{on} (V)[h]	Φ_B(meV)[i]	RR[j]	R_{ph} (A/W)[k]	
											@4.5 V	@ 4.5 V
120	31	38	350	56	Dark	5.16	6.37×10^{-7}	0.56	0.650	5.40	11.56	16.28
					Light	5.71	1.35×10^{-5}	0.06	0.570	1.15		
90	43	51	430	65	Dark	5.60	5.59×10^{-8}	2.35	0.713	1.95	0.267	0.372
					Light	5.56	2.16×10^{-7}	1.46	0.678	1.27		
60	50	60	480	74	Dark	6.05	3.23×10^{-8}	3.84	0.727	1.79	0.058	0.061
					Light	6.71	1.65×10^{-7}	2.50	0.685	1.42		

[a] Nanorod growth temperature.
[b] Crystallite size of ZnO measured from XRD.
[c] Diameter of nanorods estimated form SEM.
[d] Thickness of nanorod thin film.
[e] Inter-nanorod spacing.
[f] Diode ideality factor.
[g] Reverse saturation current.
[h] Diode turn-on voltage.
[i] Interfacial barrier height.
[j] Rectification ratio.
[k] Photocurrent responsivity.

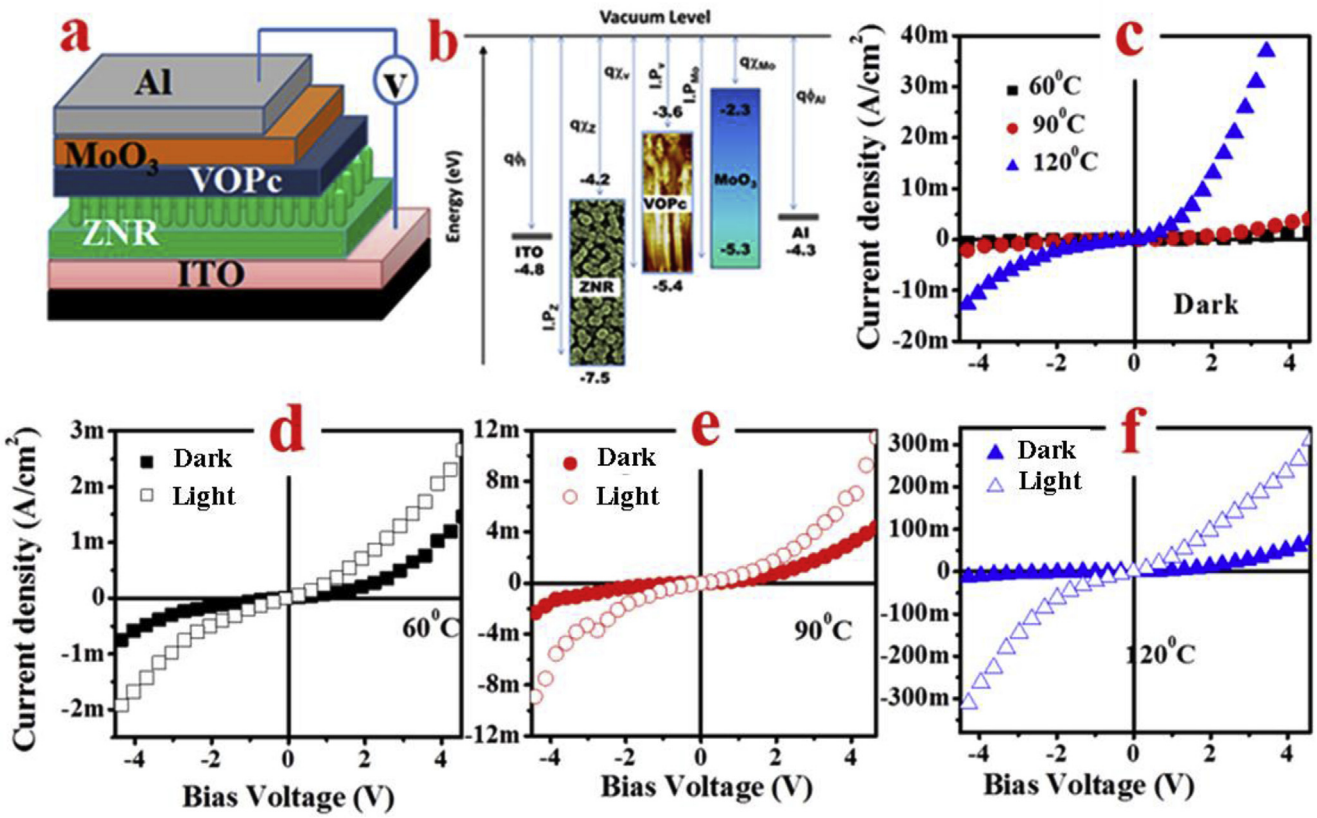

Fig. 3. (a) Schematic of the fabricated hybrid diode, **(b)** the energy level diagram for various layers in the fabricated device, **(c)** J-V characteristics of devices under dark and (d–f) J-V characteristics of the hybrid diodes under dark and illumination at a given ZNR growth temperature.

temperatures under dark condition are shown in Fig. 3(c). The characteristic diode equation under forward bias is given by Ref. [43].

$$I = I_0 exp\left(\frac{V}{nV_t}\right) \quad (1)$$

here, V_t is the thermal energy at 300 K (26 meV), V is the applied bias voltage, n is ideality factor of the diode, I_0 is the reverse saturation current and can be expressed as [9].

$$I_0 = AA^*T^2 exp\left(\frac{q\varphi_B}{kT}\right) \quad (2)$$

here, A is the area of the device (1.6 x 10^{-2}cm^2), T is the absolute temperature in K, A* is the effective Richardson's constant (32 Am^{-2}K^{-2}) for ZnO, $q\varphi_B$ is the barrier height (eV), k is the Boltzmann constant.

All the diodes exhibit rectification behaviour and the rectification ratio (RR) increased from 1.79 to 5.40 as the ZNR films growth temperature increases. On fitting the experimental data of J-V curves of ZNR films, grown at different temperatures, to the diode equation, it was found that the value of the ideality factor (n) reduces with the increase of growth temperature. It is also found that the n values are relatively higher, ranging from 6.71 to 5.16 than the ideal diode (n = 1). This may be due to the depletion region of ZNR/VOPc suffers from the electron-hole recombination, leading to a decrease in the series resistance of the device [44–46].

From Fig. 3 (c), it is seen that the current density of the device is higher for the devices with ZNR films grown at higher temperatures (120 °C). As mentioned earlier, higher growth temperatures lead to increased ZNR crystallite size (from 31 nm to 50 nm, from XRD data), and also to lowering of the interfacial barrier height from 727 meV to 650 meV (estimated using Eqs. (1) and (2)). This might be one of the reasons for high current density through devices having ZNR films grown at higher temperatures 120 °C. Correspondingly, the turn-on voltage of the diodes was reduced from 3.84 V to 0.56 V with increasing ZNR growth temperature (presented in Table 1). Further, the current density through the ZNR films (Fig. 3(c)) is found to be two orders higher in magnitude than that for the devices with nanoparticle ZnO films [6]. This can be attributed to the higher crystallite size, the larger diameter of the nanorods, and to the higher donor-acceptor interfacial area due to the filling of gaps between the nanorods by VOPc (as the gaps observed from Figure (1)).

Fig. 3(d–f) displays the J-V characteristics in dark condition and with illumination for the devices with ZNR films grown at different temperatures. It is evident that all the samples show photoresponse. The charge transfer mechanism is shown in Fig. 4. However, the photocurrent and hence the photocurrent responsivity, $R_{ph,}$ (for both forward

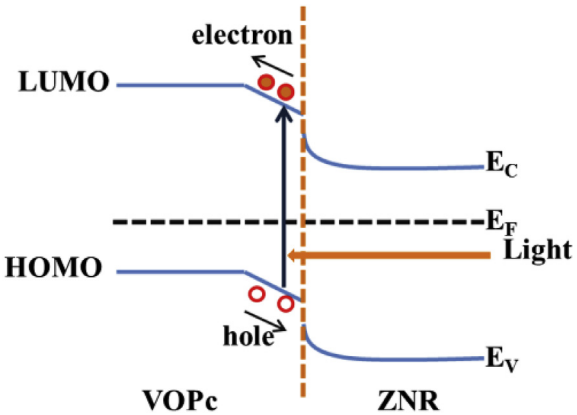

Fig. 4. Illustration of photocurrent generation mechanism in ZNR/VOPc hybrid diodes.

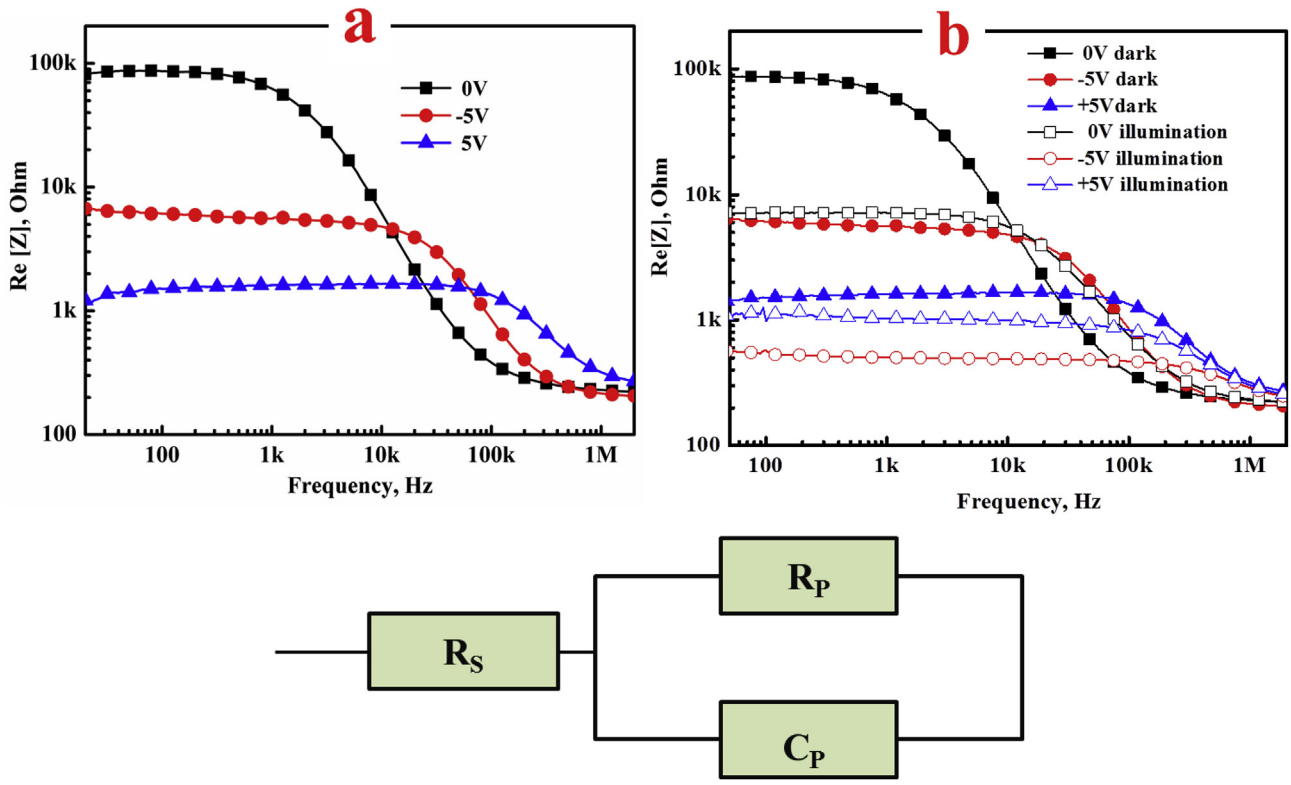

Fig. 5. (a) J-V characteristics of the hybrid diode under dark condition for ZNR films grown at 120 °C and **(b)** J-V characteristics of the hybrid diode in both dark and under illumination conditions, and (c) equivalent circuit for estimating impedance parameters. The plots in different colours represent the data for different bias voltages, as indicated in the graphs. (For interpretation of the references to colour in this figure legend, the reader is referred to the Web version of this article.)

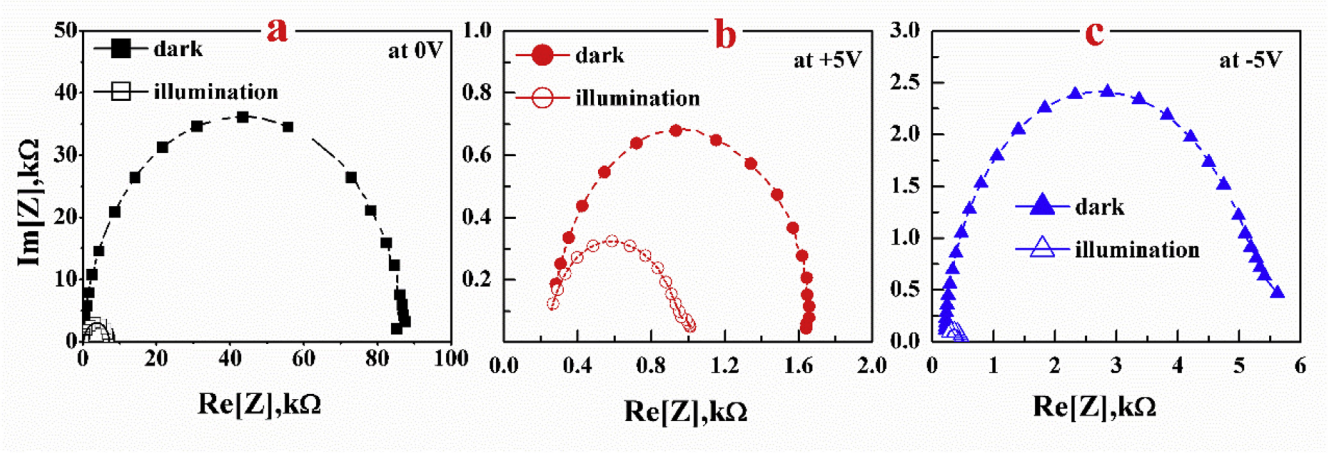

Fig. 6. Cole-Cole plots for the devices, made using ZNR, in both dark and illuminated conditions **(a)** at 0 V, **(b)** at +5 V and **(c)** -5 V.

Table 2
Estimated parameters from IS measurements employing equivalent circuit.

Parameter	at 0 V		at +5 V		at -5 V	
	Dark	Illumination	Dark	Illumination	Dark	Illumination
$R_s(\Omega)$[a]	209	201	210	221	161	223
R_P (Ω)[b]	87121	7050	1475	745	5266	264
CPE (F)[c]	2.1×10^{-9}	3.0×10^{-9}	1.2×10^{-9}	2.9×10^{-9}	1.9×10^{-9}	3.0×10^{-9}

[a] Series resistance.
[b] Parallel resistance.
[c] Constant phase element, which analogous to the parallel capacitance.

and reverse bias voltages) is higher for the devices with ZNR grown at 120 °C than the other temperatures. From Table 1, it is seen that the value of R_{ph} increased from 0.058 A/W to 11.56 A/W (200 times) under reverse bias and from 0.06 A/W to 16.28 A/W (270 times) under forward bias with the ZNR growth temperature. The R_{ph} value, for devices having ZNR films grown at 120 °C, is approximately 25 times and 125 times higher than that for the devices made using ZnO nanoparticle films under forward and reverse bias voltages (at 4.5 V), respectively [6]. It can be ascribed to the lower electron-hole recombination due to the highly efficient electron transport pathways (provided by nanorods) and, hence, better charge collection at the ZNR/VOPc interface [47].

3.4. IS measurements

To further investigate the photoresponse and the charge carrier dynamics at the hybrid heterojunctions, IS measurements were carried out for the p-n junction diode made with ZNR grown at 120 °C. Fig. 5(a) shows the resistance (Re[z]) - frequency plots for the devices in the dark conditions. From these plots, it is noted that the resistance of the devices reduces with increase in applied bias (both positive and negative). The resistance of the devices at 50 Hz was found to reduce from ~86 kΩ to ~1.48 kΩ in the forward bias (0–5 V) and ~87 kΩ–6.2 kΩ in reverse bias (0 to -5 V) voltages, respectively. The ratio of resistance (absolute value) in the reverse bias to the resistance in the forward bias, which is a measure of the rectification ratio, is found to be ~4.2. Fig. 5(b) shows the photoresponse of the devices under forward and reverse bias conditions. Upon illumination, it is seen that the bulk resistance of the devices drops remarkably at any given bias voltage. The resistance is found to be reduced from 87 kΩ to 7.1 kΩ, 1.5 kΩ–1 kΩ and 6.2 kΩ–0.6 kΩ for 0 V, +5 V and -5 V, respectively.

Fig. 6 shows the Cole-Cole plots for the devices in dark and illuminated conditions at a given bias. For each bias voltage in the dark condition, the Cole-Cole plot displays a single semicircle, which is an indication of the dominance of a single carrier lifetime. Usually, two semicircles are expected for a junction involving two materials at a given bias. Since the bulk resistance of the ZNR film (< 200 Ω) is minimal compared to the bulk resistance of VOPc (2 MΩ), the Cole-Cole plot corresponding to ZnO film is not observed in the measured range (50 Hz to 2 MHz). To analyze further, these Cole-Cole plots, equivalent circuit models, were employed similar to the one shown in Fig. 5(c). Further, it is also observed that Cole-Cole plots deviate from perfect semicircles at very low frequencies (~50 Hz) in Fig. 6(b and c), which may be due to charge accumulation at the metal/organic interface. These charges are either injected due to higher bias voltages and/or generated upon illumination.

In general, upon illumination, the following two processes are expected to occur: (i) the bulk resistance of the devices decrease due to the high photogenerated charge carrier density, and (ii) the capacitance of the devices increases due to photogenerated charge carriers [48]. We also note that the radius of the semicircle (Cole-Cole plot) for the devices at any bias is found to be reduced for measurements done under illumination. This indicates a reduction in bulk resistance under illumination. It is also observed that the capacitance of the devices increases under illumination. The values are presented in Table 2. Therefore, the high photocurrent and photoresponse for the devices with ZNR grown at 120 °C can be attributed to the improved exciton dissociation at the ZNR/VOPc interface, and to better charge collection facilitated by the vertically aligned nanorods.

4. Conclusions

In summary, several hybrid diode devices, with configuration ITO/ZNR/VOPc/MoO_3/Al, were investigated for their optoelectronic properties by varying the growth temperature of ZNR films. The interface parameters such as ideality factor (n), the Schottky barrier height ($q\varphi_B$) and the rectification ratio (RR) of the devices were determined from J-V characteristics. It was observed that the devices with the ZNR films grown at 120 °C show higher photocurrent responsivity, $R_{ph,}$ (16.28 A/W). This value is 25 times higher than the R_{ph} value obtained for the devices made with ZnO nanoparticle films. This can be attributed to the highly crystalline vertically align nanorods that can provide better pathways for charge transport. IS measurements also revealed that the high photocurrent and photoresponse for the devices with ZNR grown at 120 °C could be attributed to the improved exciton dissociation at the ZNR/VOPc interface, and to better charge collection facilitated by the vertically aligned nanorods. Hence, ZNR films annealed at 120 °C are suitable for organic-inorganic hybrid optoelectronic device applications.

Declaration of competing interest

The authors declare that they have no known competing financial interests or personal relationships that could have appeared to influence the work reported in this paper.

Acknowledgements

The Authors thank Department of Physics, National Institute of Technology Karnataka, Surathkal, India for various facilities and financial support.

Appendix A. Supplementary data

Supplementary data to this article can be found online at https://doi.org/10.1016/j.optmat.2019.109348.

References

[1] O.A. Al-Hartomy, R.K. Gupta, A.A. Al-Ghamdi, F. Yakuphanoglu, High performance organic-on-inorganic hybrid photodiodes based on organic semiconductor-graphene oxide blends, Synth. Met. 195 (2014) 217–221, https://doi.org/10.1016/j.synthmet.2014.06.001.
[2] W. Luo, L. Yan, R. Liu, T. Zou, S. Zhang, C. Liu, Q. Dai, J. Chen, H. Zhou, High detectivity ITO/organolead halide perovskite Schottky photodiodes, Semicond. Sci. Technol. 34 (2019) 74004, https://doi.org/10.1088/1361-6641/ab075d.
[3] Y.H. Lee, M. Ha, I. Song, J.H. Lee, Y. Won, S. Lim, H. Ko, J.H. Oh, High-Performance Hybrid Photovoltaics with Efficient Interfacial Contacts between Vertically Aligned ZnO Nanowire Arrays and Organic Semiconductors, ACS Omega 4 (2019) 9996–10002, https://doi.org/10.1021/acsomega.9b00778.
[4] J. Dar Hwang, C. Wei Fan, High-performance organic/inorganic hybrid ultraviolet p-NiO/PVK/n-ZnO heterojunction photodiodes with a poly(N -vinylcarbazole) insertion layer, J. Mater. Chem. C. 7 (2019) 3529–3534, https://doi.org/10.1039/C8TC04950E.
[5] F. Aslan, H. Esen, F. Yakuphanoglu, Electrical and fotoconducting characterization of Al/coumarin:ZnO/Al novel organic-inorganic hybrid photodiodes, J. Alloys Compd. 789 (2019) 595–606, https://doi.org/10.1016/j.jallcom.2019.03.090.
[6] M.R. Kiran, H. Ulla, M.N. Satyanarayan, G. Umesh, Optoelectronic properties of hybrid diodes based on vanadyl-phthalocyanine and zinc oxide, Superlattice Microstruct. 112 (2017) 654–664, https://doi.org/10.1016/j.spmi.2017.10.023.
[7] G.D. Sharma, R. Kumar, S.K. Sharma, M.S. Roy, Charge generation and photovoltaic properties of hybrid solar cells based on ZnO and copper phthalocyanines (CuPc), Sol. Energy Mater. Sol. Cells 90 (2006) 933–943, https://doi.org/10.1016/j.solmat.2005.05.012.
[8] R.K. Gupta, F. Yakuphanoglu, K. Ghosh, P.K. Kahol, Fabrication and characterization of p–n junctions based on ZnO and CuPc, Microelectron. Eng. 88 (2011) 3067–3069, https://doi.org/10.1016/j.mee.2011.05.023.
[9] Z. Yuan, A photodiode with high rectification ratio and low turn-on voltage based on ZnO nanoparticles and SubPc planar heterojunction, Phys. E Low-Dimens. Syst. Nanostructures. 56 (2014) 160–164, https://doi.org/10.1016/j.physe.2013.09.001.
[10] Z. Yuan, M. Fu, Y. Ren, Optoelectronic properties of ZnO nanoparticle/pentacene heterojunction photodiode, J. Electron. Mater. 43 (2014) 3270–3275, https://doi.org/10.1007/s11664-014-3268-1.
[11] A. Pickett, A. Mohapatra, A. Laudari, S. Khanra, T. Ram, S. Patil, S. Guha, Hybrid ZnO-organic semiconductor interfaces in photodetectors: a comparison of two near-infrared donor-acceptor copolymers, Org. Electron. 45 (2017) 115–123, https://doi.org/10.1016/j.orgel.2017.03.001.
[12] Y. Xi, J. Song, S. Xu, R. Yang, Z. Gao, C. Hu, Z.L. Wang, Growth of ZnO nanotube arrays and nanotube based piezoelectric nanogenerators, J. Mater. Chem. 19 (2009) 9260–9264, https://doi.org/10.1039/B917525C.
[13] J. Huang, Z. Yin, Q. Zheng, Applications of ZnO in organic and hybrid solar cells, Energy Environ. Sci. 4 (2011) 3861–3877, https://doi.org/10.1039/C1EE01873F.
[14] K.W. Jeong, H.S. Kim, G.R. Yi, C.K. Kim, Enhancing the electroluminescence of

OLEDs by using ZnO nanoparticle electron transport layers that exhibit the Auger electron effect, Mol. Cryst. Liq. Cryst. 663 (2018) 61–70, https://doi.org/10.1080/15421406.2018.1468099.
[15] O. Ostroverkhova, Organic Optoelectronic Materials: Mechanisms and Applications, Chem. Rev. 116 (2016) 13279–13412, https://doi.org/10.1021/acs.chemrev.6b00127.
[16] R.D. Gould, Structure and electrical conduction properties of phthalocyanine thin films, Coord. Chem. Rev. 156 (1996) 237–274.
[17] R.D. Gould, A.K. Hassan, A.c. electrical properties of thermally evaporated thin films of copper phthalocyanine, Thin Solid Films 223 (1993) 334–340, https://doi.org/10.1016/0040-6090(93)90541-V.
[18] T.D. Anthopoulos, T.S. Shafai, Alternating current conduction properties of thermally evaporated α-nickel phthalocyanine thin films: effects of oxygen doping and thermal annealing, J. Appl. Phys. 94 (2003) 2426–2433.
[19] T.S. Shafai, T.D. Anthopoulos, Junction properties of nickel phthalocyanine thin film devices utilising indium injecting electrodes, Thin Solid Films 398 (2001) 361–367.
[20] H.R. Pekbelgin Karaoğlu, A. Gül, M.B. Koçak, Synthesis and characterization of a new tetracationic phthalocyanine, Dyes Pigments 76 (2008) 231–235, https://doi.org/10.1016/j.dyepig.2006.08.032.
[21] S. Kaipova, H. Dinçer, A. Altindal, Synthesis, characterization, conduction, and dielectric properties of tetra tert-butylsulfanyl substituted phthalocyanines, J. Coord. Chem. 68 (2015) 717–731, https://doi.org/10.1080/00958972.2014.992340.
[22] T. Sakurai, T. Ohashi, H. Kitazume, M. Kubota, T. Suemasu, K. Akimoto, Structural control of organic solar cells based on nonplanar metallophthalocyanine/C60 heterojunctions using organic buffer layers, Org. Electron. 12 (2011) 966–973, https://doi.org/10.1016/j.orgel.2011.03.016.
[23] J. Kim, S. Yim, Influence of surface morphology evolution of SubPc layers on the performance of SubPc/C60 organic photovoltaic cells, Appl. Phys. Lett. 99 (2011) 193303, https://doi.org/10.1063/1.3660710.
[24] J. Kim, S. Yim, Influence of surface morphology evolution of SubPc layers on the performance of SubPc/C60 organic photovoltaic cells, Appl. Phys. Lett. 99 (2011) 193303, https://doi.org/10.1063/1.3660710.
[25] G. Williams, S. Sutty, R. Klenkler, H. Aziz, Renewed interest in metal phthalocyanine donors for small molecule organic solar cells, Sol. Energy Mater. Sol. Cells 124 (2014) 217–226, https://doi.org/10.1016/j.solmat.2014.02.013.
[26] D. Song, F. Zhu, B. Yu, L. Huang, Y. Geng, D. Yan, Tin (IV) phthalocyanine oxide: an air-stable semiconductor with high electron mobility, Appl. Phys. Lett. 92 (2008) 143303, https://doi.org/10.1063/1.2903486.
[27] F. Jin, B. Chu, W. Li, Z. Su, X. Yan, J. Wang, R. Li, B. Zhao, T. Zhang, Y. Gao, C.S. Lee, H. Wu, F. Hou, T. Lin, Q. Song, Highly efficient organic tandem solar cell based on SubPc:C70 bulk heterojunction, Org. Electron. 15 (2014) 3756–3760, https://doi.org/10.1016/j.orgel.2014.10.019.
[28] L. Li, Q. Tang, H. Li, X. Yang, W. Hu, Y. Song, Z. Shuai, W. Xu, Y. Liu, D. Zhu, An ultra closely π-stacked organic semiconductor for high performance field-effect transistors, Adv. Mater. 19 (2007) 2613–2617, https://doi.org/10.1002/adma.200700682.
[29] G. Mattioli, C. Melis, G. Malloci, F. Filippone, P. Alippi, P. Giannozzi, A. Mattoni, A. Amore Bonapasta, Zinc Oxide–Zinc Phthalocyanine Interface for Hybrid Solar Cells, J. Phys. Chem. C. 116 (2012) 15439–15448, https://doi.org/10.1021/jp303781v.
[30] Y. Yoshida, M. Nakamura, S. Tanaka, I. Hiromitsu, Y. Fujita, K. Yoshino, Photovoltaic properties and inner electric field of ZnO/Zn-phthalocyanine hybrid solar cells, Synth. Met. 156 (2006) 1213–1217, https://doi.org/10.1016/j.synthmet.2006.09.001.
[31] B. Singh, A. Sharma, S. Ghosh, Current transport mechanism in ZnO and metal phthalocyanine based inorganic/organic hybrid p–n junction diodes, J. Electron. Mater. 47 (2018) 5595–5600, https://doi.org/10.1007/s11664-018-6467-3.
[32] Q. Chen, H. Ding, Y. Wu, M. Sui, W. Lu, B. Wang, W. Su, Z. Cui, L. Chen, Passivation of surface states in the ZnO nanowire with thermally evaporated copper phthalocyanine for hybrid photodetectors, Nanoscale 5 (2013) 4162–4165, https://doi.org/10.1039/C3NR01088K.
[33] B. Singh, S. Ghosh, Zinc oxide and metal phthalocyanine based hybrid P-N junction diodes, Appl. Phys. Lett. 103 (2013) 133301, https://doi.org/10.1063/1.4821780.
[34] X. Luo, L. Xu, B. Xu, F. Li, Electrodeposition of zinc oxide/tetrasulfonated copper phthalocyanine hybrid thin film for dye-sensitized solar cell application, Appl. Surf. Sci. 257 (2011) 6908–6911, https://doi.org/10.1016/j.apsusc.2011.03.029.
[35] P.I. Stakhira, G.L. Pakhomov, V.V. Cherpak, D. Volynyuk, G. Luka, M. Godlewski, E. Guziewicz, Z.Y. Hotra, Photovoltaic cells based on nickel phthalocyanine and zinc oxide formed by atomic layer deposition, Cent, Eur. J. Phys. 8 (2010) 798–803, https://doi.org/10.2478/s11534-009-0159-9.
[36] A. Kumar, S. Samanta, A. Singh, M. Roy, S. Singh, S. Basu, M.M. Chehimi, K. Roy, N. Ramgir, M. Navaneethan, Y. Hayakawa, A.K. Debnath, D.K. Aswal, S.K. Gupta, Fast response and high sensitivity of ZnO nanowires—cobalt phthalocyanine heterojunction based H2S sensor, ACS Appl. Mater. Interfaces 7 (2015) 17713–17724, https://doi.org/10.1021/acsami.5b03652.
[37] M.R. Kiran, H. Ulla, M.N. Satyanarayan, G. Umesh, Effect of deposition rate on the charge transport in Vanadyl-phthalocyanine thin films, Synth. Met. 224 (2017) 63–71, https://doi.org/10.1016/j.synthmet.2016.12.025.
[38] M.R. Kiran, H. Ulla, J.M. Fernandes, M.N. Satyanarayan, G. Umesh, Electrical characterization of hybrid hetero interface using n-ZnO and p-CuPc, Mater. Today Proc. 2 (2015) 1230–1233, https://doi.org/10.1016/j.matpr.2015.07.036.
[39] A. Henni, A. Merrouche, L. Telli, A. Karar, Studies on the structural, morphological, optical and electrical properties of Al-doped ZnO nanorods prepared by electrochemical deposition, J. Electroanal. Chem. 763 (2016) 149–154, https://doi.org/10.1016/j.jelechem.2015.12.037.
[40] E. Kärber, T. Raadik, T. Dedova, J. Krustok, A. Mere, V. Mikli, M. Krunks, Photoluminescence of spray pyrolysis deposited ZnO nanorods, Nanoscale Res. Lett. 6 (2011) 359, https://doi.org/10.1186/1556-276X-6-359.
[41] A. Subrahmanyam, K.P. Biju, P. Rajesh, K. Jagadeesh Kumar, M. Raveendra Kiran, Surface modification of sol gel TiO2 surface with sputtered metallic silver for Sun light photocatalytic activity: initial studies, Sol. Energy Mater. Sol. Cells 101 (2012) 241–248, https://doi.org/10.1016/j.solmat.2012.01.023.
[42] M.R. Kiran, H. Ulla, M.N. Satyanarayan, G. Umesh, Optoelectronic properties of hybrid diodes based on vanadyl-phthalocyanine and zinc oxide, Superlattice Microstruct. 112 (2017) 654–664, https://doi.org/10.1016/j.spmi.2017.10.023.
[43] F.T. Reis, D. Mencaraglia, S. Ould Saad, I. Séguy, M. Oukachmih, P. Jolinat, P. Destruel, Electrical characterization of ITO/CuPc/Al diodes using temperature dependent capacitance spectroscopy and I–V measurements, J. Non-Cryst. Solids (2004) 338–340, https://doi.org/10.1016/j.jnoncrysol.2004.03.050 599–602.
[44] S. Darwish, A.S. Riad, H.S. Soliman, Electrical conductivity and the effect of temperature on photoconduction of n-ZnSe/p-Si rectifying heterojunction cells, Semicond. Sci. Technol. 11 (1996) 96–102, https://doi.org/10.1088/0268-1242/11/1/021.
[45] K. Mayes, A. Yasan, R. McClintock, D. Shiell, S.R. Darvish, P. Kung, M. Razeghi, High-power 280 nm AlGaN light-emitting diodes based on an asymmetric single-quantum well, Appl. Phys. Lett. 84 (2004) 1046–1048, https://doi.org/10.1063/1.1647273.
[46] A. Dey, A. Layek, A. Roychowdhury, M. Das, J. Datta, S. Middya, D. Das, P.P. Ray, Investigation of charge transport properties in less defective nanostructured ZnO based Schottky diode, RSC Adv. 5 (2015) 36560–36567, https://doi.org/10.1039/C4RA16828C.
[47] I. Gonzalez-Valls, M. Lira-Cantu, Vertically-aligned nanostructures of ZnO for excitonic solar cells: a review, Energy Environ. Sci. 2 (2008) 19–34, https://doi.org/10.1039/B811536B.
[48] S. Hamza, A. Mhamdi, W. Aloui, A. Bouazizi, K. Khirouni, Effect of illumination on the dielectrical properties of P3HT:PC70BM nanocomposites, Mater. Res. Express 4 (2017) 055003, , https://doi.org/10.1088/2053-1591/aa6ac1.